Synchrotron-radiation-excited angle-resolved photoemission from single-crystal graphite

A. R. Law, M. T. Johnson, and H. P. Hughes
Cavendish Laboratory, University of Cambridge, Madingley Road, Cambridge, CB3 0HE, Cambridgeshire, England, United Kingdom
(Received 29 July 1985)

Synchrotron-radiation-excited angle-resolved photoemission from a single crystal of natural graphite is reported. Using photon energies between 20 and 65 eV, all the valence-band dispersions and critical-point binding energies have been determined. The photon-energy dependence of normal emission spectra yielded a π-band k_z dispersion of ~ 1 eV, less than theoretically predicted. Distinct secondary-electron features in the spectra allow determination of the dispersion of certain conduction bands lying up to 20 eV above the Fermi level. Such high-energy conduction bands have not been observed by inverse photoemission.

I. INTRODUCTION

The two-dimensional crystal structure of graphite has made it an attractive subject for experimental and theoretical study. The stable form of graphite is that in which the planar hexagonal networks of carbon atoms are stacked in an *ABABA* sequence. Half the carbon atoms are located directly above each other in adjacent planes and half are located above the centers of the hexagons in the adjacent planes. Assuming the hexagonal planes are exactly planar, this crystal structure belongs to the space group $P6_3/mmc$ (D_{6h}^4) with four atoms per unit cell.

Bonding within the layers is strong and is conveniently described by sp^2 hybridized $2s$, $2p_x$, and $2p_y$ atomic orbitals. The bonding between the layers is weak, originating from the overlap between $2p_z$ orbitals. Theoretical band structures have been calculated by various computational techniques (Ref. 1, and references therein), many of which have neglected the weak interlayer interaction and calculated the band structure for a single graphite layer. The resulting band structure consists of a bonding manifold of one π band and three σ bands, forming the filled valence band, above which lies the conduction band consisting of the corresponding antibonding π^* and σ^* bands. Including the interlayer interaction in a three-dimensional calculation results in a splitting of the bands across the $K\Gamma M$ plane of the Brillouin zone (shown in Fig. 1). This splitting is greatest for the π bands, for which the interlayer orbital overlap is greatest.

Experimental aspects of the band structure have been studied by x ray[2] and ultraviolet excited photoemission,[3–8] inverse photoemission,[9,10] secondary-electron emission,[11,12] electron energy loss,[13] and optical measurements.[14] These studies have employed both natural single crystals of graphite and turbostratically disordered highly oriented pyrolytic graphite (HOPG) samples.

We have previously reported angle-resolved ultraviolet photoemission spectroscopy (ARUPS) from a single crystal of natural graphite, obtained using He I light ($h\nu=21.2$ eV) from a standard gas discharge source.[5] In this paper we present new results obtained using the Synchrotron Radiation Source at the SERC Daresbury Labo-

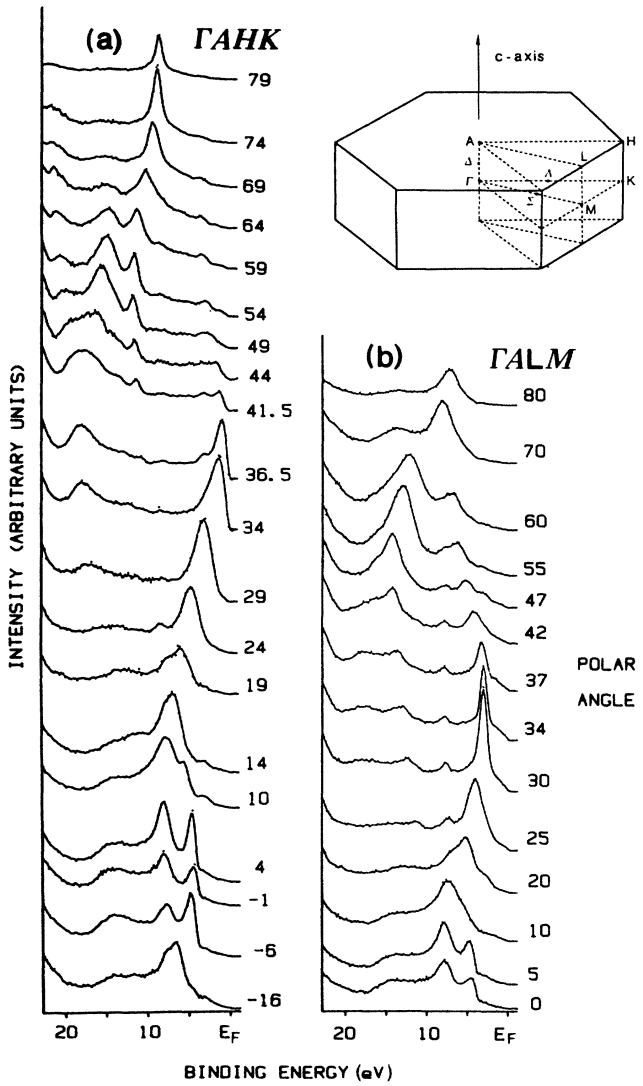

FIG. 1. Energy distribution curves obtained for (a) the ΓAHK plane and (b) the ΓALM plane with $h\nu=35$ eV. The secondary-electron tail has been omitted for clarity. The Brillouin zone of graphite, giving the critical-point notation used here, is also shown,.

ratory. Brief experimental details in Sec. II are followed in Sec. III by presentation and discussion of ARUPS results for photon energies of 35 and 65 eV. In Sec. IV spectra obtained at normal emission, and as a function of photon energy, showing the π-band dispersion normal to the layers, are presented. Finally, in Sec. V, the data are compared with various theoretical band-structure calculations.

II. EXPERIMENTAL DETAILS

The experiments reported here were performed using the VG Scientific ADES 400 spectrometer on beam line 6 at the Synchrotron Radiation Source at the Daresbury Laboratory.

Electrons were energy analyzed using a spherical sector analyzer having angular acceptance $\pm 2°$ and typical energy resolution ± 0.2 eV. The light was p-polarized [(with electric vector E in the plane of incidence (and detection)] and the photon energy was varied (10 eV $< h\nu <$ 65 eV) using a toroidal grating monochromator operated at an energy resolution of ± 0.1 eV.

The natural graphite single crystal was cleaved immediately prior to insertion into the vacuum chamber and subsequently cleaned *in situ* by electron bombardment heating to ~ 1500 °C, until ultraviolet photoemission spectroscopy (UPS) spectra characteristic of a clean sample were obtained. The monocrystalline nature of the sample was confirmed by low-energy electron diffraction (LEED) which also enabled the azimuthal orientation of the sample to be determined unambiguously. The experiments were performed at a base pressure of 10^{-10} Torr.

III. EXPERIMENTAL RESULTS

As can be seen from our earlier paper,[5] He I light (21.2 eV) is not sufficiently energetic to excite electrons from the whole width of the valence band to states above the vacuum level, or to allow the dispersion of higher binding energy bands to be followed out to the edges of the first Brillouin zone. (Throughout this paper binding energies are relative to the Fermi level, E_F.) Also, certain bands, for example, the highly dispersive σ valence band in the ΓALM plane (σ_2 in Fig. 2), were not observed. This absence was attributed to the low joint density of states (JDOS) resulting from the opposite gradient of the final state involved for a photon energy of 21.2 eV. Using a photon energy of 35 eV electrons from this band, and indeed from all the valence bands, should be excited into regions where the calculated final states of the Tatar and Rabii band structure[1] have a similar gradient to the initial states. This modified Korringa-Kohn-Rostoker (KKR) band-structure calculation has already been shown by the He I data[5] to be essentially correct.

Figure 1 shows energy distribution curves (EDC's) obtained for the ΓAHK and ΓALM azimuths using photons of energy 35 eV, incident at 45° to the sample normal. Features in the spectra are reduced in the usual way[15] to an initial-state energy E_i versus parallel component of momentum $k_{||}$ diagram (Fig. 2). Superimposed on the experimental data are the initial-state bands of the Tatar and Rabii (TR) band structure.[1] For the earlier He I data the theoretical bands were rigidly shifted down by around 0.5 eV to give best qualitative agreement between theory and experiment. Such a shift can be attributed to a very small concentration of impurities raising the Fermi level E_F up through the conduction bands. No such shift has been applied here.

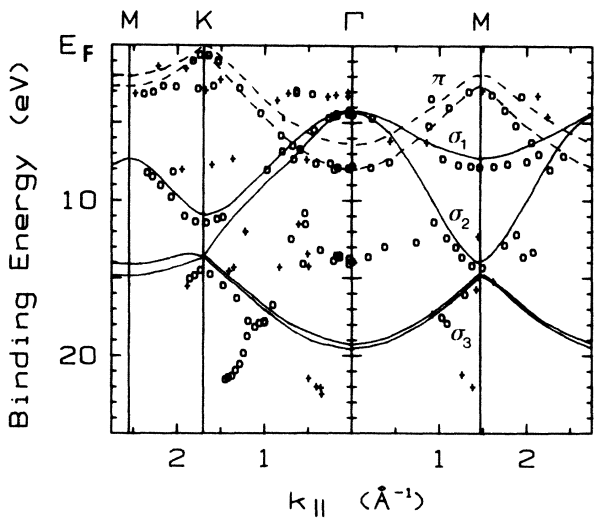

FIG. 2. Features in the 35 eV spectra shown in Fig. 1 reduced to an initial-state binding energy versus $k_{||}$ diagram. o, strong or distinct features; +, weak features. Superimposed are the calculated valence bands of Ref. 1; ——, σ bands; — — —, π bands.

As with the He I data, the spectra show features that can be attributed to secondary-electron emission (SEE). To determine the conduction bands involved, the data were replotted on a kinetic energy (KE) versus $k_{||}$ diagram and compared with the theoretical TR conduction bands (Fig. 3). (The conduction bands have been calculated only up to 28 eV above the Fermi level.) Also plotted in Fig. 3 are features observed in the secondary-electron tail of the spectra. (The secondary tails are omitted from Fig. 1 for clarity.) Of these the strongest occurs at ~ 3 eV kinetic energy above the vacuum energy and shows no dispersion. The energy of the weak, nondispersing feature at 6 eV KE was determined by differentiation of the spectra. From this figure it is clear that features not related to valence bands in Fig. 2 arise from emission from certain conduction bands. To lift the valence-band region clear of the conduction bands giving rise to these strong secondary-electron features, the photon energy was increased to 65 eV.

Figure 4 shows EDC's obtained in the ΓAHK plane using 65 eV photons incident at 45°. Features in these spectra are reduced to an E_i versus $k_{||}$ diagram and compared with the TR calculation in Fig. 5. As expected, the valence-band region now shows no secondary-electron features, these appearing at lower kinetic energies. The higher photon energy also allows the valence-band dispersions to be followed further out in k space. Distinct, dispersing secondary-electron features appearing in the spectra between 7 and 25 eV kinetic energy are displayed

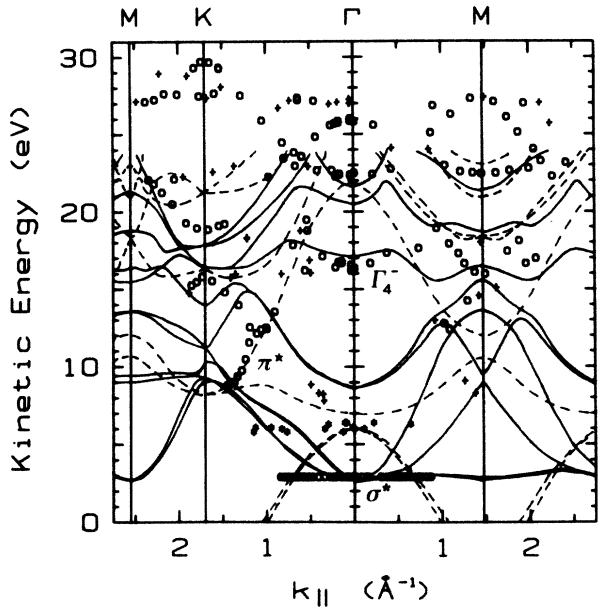

FIG. 3. Features in the 35 eV spectra replotted on a kinetic energy versus $k_{||}$ diagram, to compare with the calculated available final states (Ref. 1). ○, strong or distinct features; +, weak features; *, weak features obtained by differentiation of the spectra; ——, σ^* bands; — — —, π^* bands.

in Fig. 6 and compared with the calculated conduction bands in Fig. 7. The very strong secondary feature at ~3 eV KE is omitted from Fig. 6 but plotted in Fig. 7.

The experimentally determined valence- and conduction-band dispersions show good agreement with the calculated band structure of Tatar and Rabii.[1] Using higher photon energies the band dispersions have been followed out to, and beyond, the edges of the first Brillouin zone. Binding energies of critical points at M determined from the $h\nu=65$ eV data are consistent with those determined with $h\nu=35$ eV, giving no evidence for different correlation and/or screening effects resulting from the different photoelectron kinetic energies.

As can be seen from Fig. 1, the highly dispersive σ valence band in the ΓALM direction, σ_2, not present in the He I data, is now observed, the intensity of the feature becoming stronger as the band crosses into the second Brillouin zone; similar behavior is observed for the lowest binding energy σ band (σ_1 in Fig. 2) in the ΓAHK plane. Intensity asymmetry on crossing a zone boundary is also observed, but in an opposite sense, in the $h\nu=35$ eV data for the π band in both the ΓALM plane and, more dramatically, the ΓAHK plane. From consideration of the atomic orbitals involved in the formation of the valence bands, the intensity of emission from the σ bands ($2s, 2p_x, 2p_y$ basis orbitals) is expected to increase, and that from the π bands ($2p_z$ basis orbitals) decrease, as the polar angle is increased.[16,17] However, while contributing to the overall trend, with σ-band emission generally stronger than π-band emission at high polar angles, this effect cannot explain the sharp intensity changes observed as certain bands cross zone boundaries. Such intensity asymmetries can only be fully explained by detailed consideration of the plane-wave components of the final-state wave functions involved, and their matching at the surface to plane waves in vacuum.[16] Intensity asymmetries are also observed in the 65 eV data (Fig. 5) as, for example, with the lowest binding energy σ valence band when crossing M ($\theta=40°$).

The π-band intensity also diminishes when crossing K ($k_{||}=1.70$ Å^{-1}) but increases again at higher angles, having crossed the second K point ($k_{||}=3.40$ Å^{-1}) further out in reciprocal space. Such dramatic intensity changes at zone boundaries have also been observed in ARUPS data from other materials, e.g., copper,[18] where the asymmetric behavior was attributed to the change in sign of the reduced **k** vector of the periodic initial state, whereas the momentum of the free-electronlike final state continues smoothly across the boundary.

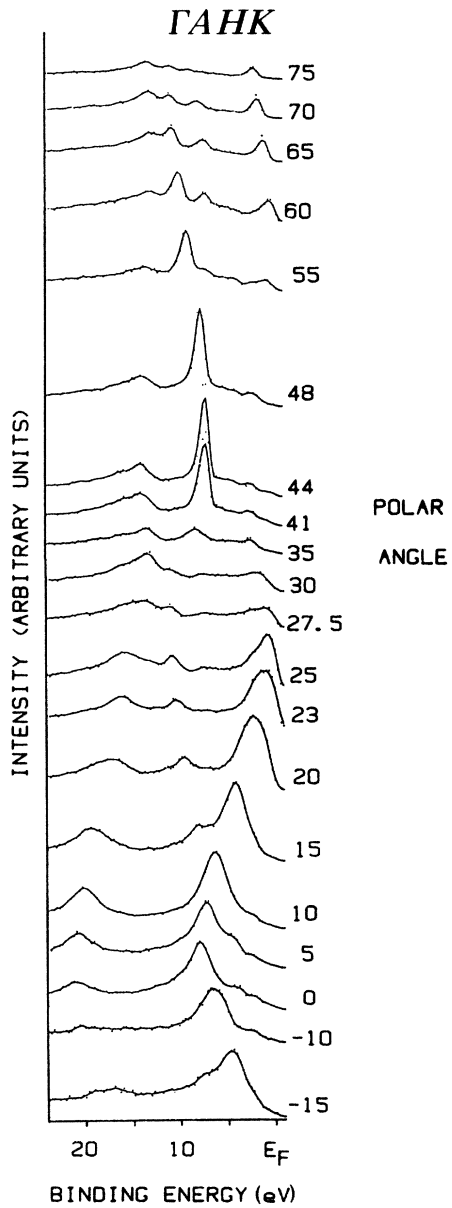

FIG. 4. Valence-band region of the EDC's recorded in the ΓAHK plane with $h\nu=65$ eV.

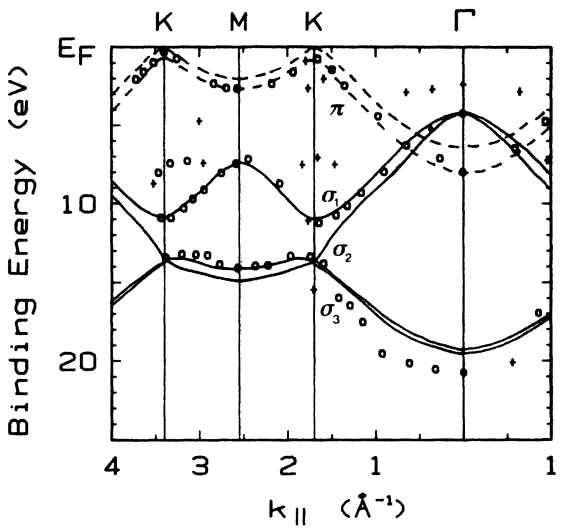

FIG. 5. Features in the 65 eV spectra plotted on a binding energy versus $k_{||}$ diagram. ○, strong or distinct features; +, weak features. Superimposed are the calculated valence bands of Ref. 1; ——, σ bands; — — —, π bands.

Hermanson[19] has discussed the symmetry of observable final states in photoemission. For emission in a mirror plane (such as that corresponding to ΓALM in real space) only final states with even parity with respect to reflection in the mirror plane can be detected. Dipole selection rules then impose a restriction on accessible initial states, depending on the polarization of the incident light. In this experiment the light is p polarized (the electric vector $\mathbf{E}$ is in the plane of incidence and detection) and hence has even parity with respect to reflection in the mirror plane. If the divergence of the vector potential $\mathbf{A}$ of the incident light is assumed to be negligible and taken as equal to zero, $\nabla\cdot\mathbf{A}=0$, the resulting bulk photoexcitation matrix element implies that only even-parity initial states should be accessible here. However, observation of emission from the odd-parity σ_1 valence band at all photon energies, together with the independence of its intensity on $k_{||}$, implies the breakdown of this bulk matrix element approximation. At the surface the vector potential will be varying rapidly, i.e., $\nabla\cdot\mathbf{A}\neq 0$, and further terms must be included in the photoexcitation matrix element to account for this divergence.[20]

The highest binding-energy valence band, σ_3 in Fig. 2, is not observed at Γ for $h\nu=35$ eV, though it is detected near K and, less distinctly, near M. It is observed, however, for $h\nu=65$ eV and lies ~ 1.5 eV to higher binding energy at Γ than calculated. Thus for $h\nu=35$ eV electrons from this band would be excited into the calculated σ^* conduction-band minimum at ~ 14 eV above E_F, lying at the bottom of a calculated gap in the conduction bands along $A\Gamma A$. Dipole selection rules, however, forbid at Γ transitions from the σ_3 band to the available final state, although they are weakly allowed along ΓK and ΓM and at A. As discussed later, no secondary-electron emission is observed from this σ^* conduction band.

From Fig. 1 it can be seen that as the π band approaches the Fermi level in both the ΓK and ΓM directions the full width at half maximum (FWHM) of the peak decreases, reflecting the expected longer hole lifetime. Also, as observed in the He I data, the intensity of π-band emission strongly increases around M, reflecting the high initial density of states.

Emission from the σ_1, σ_2 bands at Γ is much weaker for $h\nu=65$ eV than for $h\nu=35$ eV. This photon-energy dependence will be discussed further with the normal-emission data in Sec. IV.

Weak structure observed at ~ 3 eV binding energy for all photon energies used (and in the normal-emission spectra reported later in this paper), must be an initial-state feature, the kinetic energy of secondary-electron features being independent of photon energy. This feature is also observed by Marchand *et al.*[3] and by McGovern *et al.*,[6] who suggest that it could arise from a surface state or emission from isolated carbon atoms on the outermost

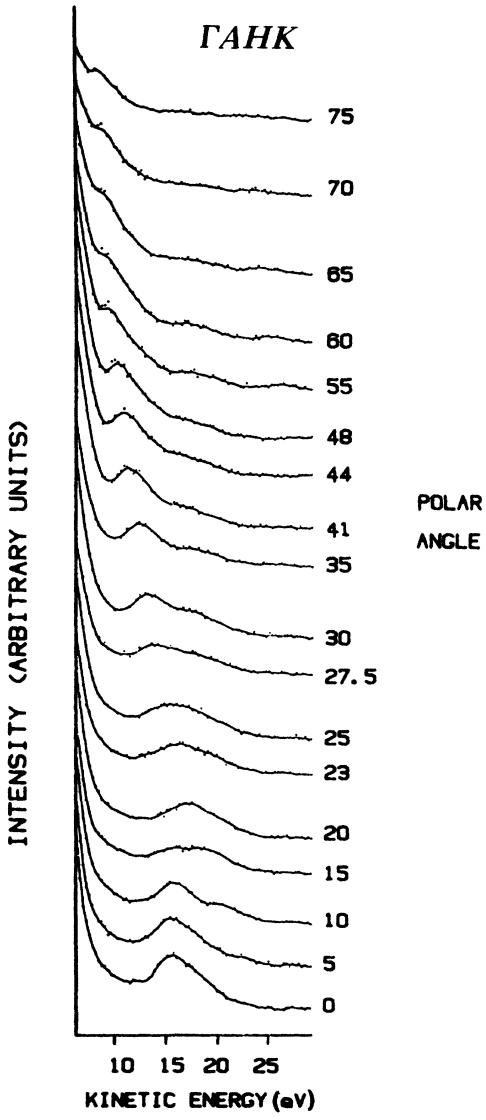

FIG. 6. Secondary-electron features appearing in the 65 eV spectra between 7 and 25 eV kinetic energy.

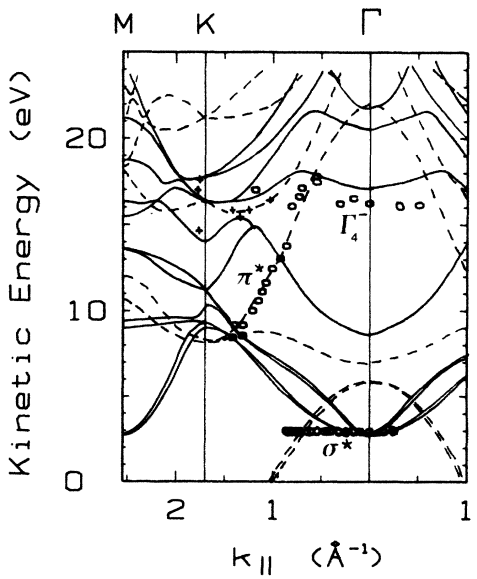

FIG 7. Features in Fig. 6 reduced to a kinetic energy versus $k_{||}$ diagram and compared with the calculated conduction bands of Ref. 1. ○, strong or distinct features; +, weak features; ——, σ^* bands; — — —, π^* bands.

plane of C atoms. Alternatively, it could result from non-k-conserving transitions from the high density-of-states region at M at that binding energy.

In the 65 eV data, a weak, yet distinct structure is observed at ~8 eV binding energy at both K points, the intensity of this feature being stronger around the second K point ($k_{||}=3.4$ Å^{-1}) than the first ($k_{||}=1.7$ Å^{-1}). This cannot be attributed to an umklapp process from the high density-of-states region at this binding energy at M since no suitable reciprocal-lattice vector exists to produce an elastic scattering from M to K. Nor can it be the result of momentum broadening (with electrons excited from the high density-of-states region at M being quasielastically scattered across to K) since the feature shows dispersion. This feature could be secondary emission from a high density of final states present at K at that final-state energy.

Three very prominent secondary-electron features are seen at both photon energies employed. The strongest SEE feature is that observed at ~3 eV KE which shows no dispersion. This has been associated within the σ^* conduction band minimum at ~7.6 eV above E_F at Γ.[11,21,22] SEE emission across the zone at around 16 eV kinetic energy (~21 eV above E_F) can be identified as arising from the fairly flat σ^* conduction band having Γ_4^- symmetry at the zone center (see Fig. 3). The third prominent SEE feature [also seen in He I data (Ref. 5)] arises from emission from the highly dispersive π^* band in the ΓK direction. Secondary-electron emission might be expected from the σ^* conduction band whose minimum at ~14 eV above the Fermi level lies at the bottom of a calculated 8-eV wide conduction-band gap. This is actually two bands of Γ_1^+ and Γ_4^- symmetry, both of which should be detectable from symmetry considerations.[23] However, no such emission is observed. Nor, indeed, as mentioned earlier, was any expected primary-electron emission observed in this region from weakly allowed transitions around Γ (though actually forbidden at Γ). Negligible dispersion in the ΓA direction is calculated for this band, whereas the observed conduction band at ~21 eV above E_F at the top of the calculated band gap shows around 2 eV dispersion.

Apparently, only conduction bands showing dispersion along ΓA give rise to the distinct secondary-electron features in the spectra. This implies that transport to the surface is favored in bands having nonzero group velocities in the ΓA direction. This idea is supported by the strongest secondary feature, that at ~3 eV kinetic energy, which corresponds to emission from the high density-of-states region lying 7.6 eV above E_F in the TR calculation, with σ^* conduction bands of Γ_1^+, Γ_5^+, and, Γ_6^- symmetry. The Γ_1^+ state, the only one with the correct symmetry to be detected,[23] is also predicted to disperse in the ΓA direction. This σ^* band corresponds to the "interlayer state" band discussed by Posternak *et al.*[24] In the TR calculation, this band appears ~4 eV higher in energy above E_F than in the calculations of Posternak *et al.*[24] and Holzwarth *et al.*[25]

In a separate paper[21] we have presented the results of a constant final-state photoemission (CFSPES) experiment that gave evidence for the existence of a conduction band having energy and $K_{||}$ dispersion along ΓM in agreement with that calculated for this band by TR. In momentum-(k-) resolved inverse photoemission (KRIPES) (Ref. 10); however, this band is observed where predicted by Ref. 25, at ~3.6 eV above E_F. No feature was observed by KRIPES at 7.6 eV above E_F, though a nondispersive feature was seen at 9.5 eV above E_F. [No secondary features were observed at this energy, though in the 35 eV data a very weak feature at 10.5 eV was determined by differentiation of the secondary tail (Fig. 3). A weak, yet distinct feature at ~10 eV above E_F was also seen in the earlier He I data (Ref. 15).] Therefore discrepancies exist between the energies of conduction bands as determined by KRIPES (Ref. 10) and by CFSPES (Ref. 21) and SEE. (In addition to the SEE results presented here and in our previous paper,[5] the strong SEE features exhibited by graphite have also been reported by many other authors, for example, Refs. 3, 4, 8, 11, 12, and 26.)

Similar discrepancies arise in the case of the first-stage lithium graphite intercalation compound, LiC_6, where KRIPES (Ref. 10) observes the σ^* conduction band minimum at 2 eV higher energy (7.6 eV above E_F) than SEE (Ref. 27) (5.6 eV above E_F).

As discussed in Refs. 21 and 22, no obvious explanation of these discrepancies presents itself, though the agreement of KRIPES with the calculation of Holzwarth *et al.*[25] while SEE and CFSPES agree with the TR calculation, suggests that clues to an explanation may lie in the nature of these different band-structure calculations. Indeed, the energy position of the lower conduction bands is very dependent on the choice of crystal potential and exchange-correlation approximation used in these and other band-structure calculations. Clearly further theoretical work is required.

IV. NORMAL EMISSION DATA

To determine the dispersion of the π valence bands in the ΓA direction, EDC's were recorded at normal emission as a function of photon energy. These spectra are shown in Fig. 8 for photon energies between 22 and 65 eV. Since the density of states at E_F is very low, determination of the position of the Fermi level in these spectra is difficult. Therefore, the spectra are calibrated with respect to the strong, nondispersing secondary feature at

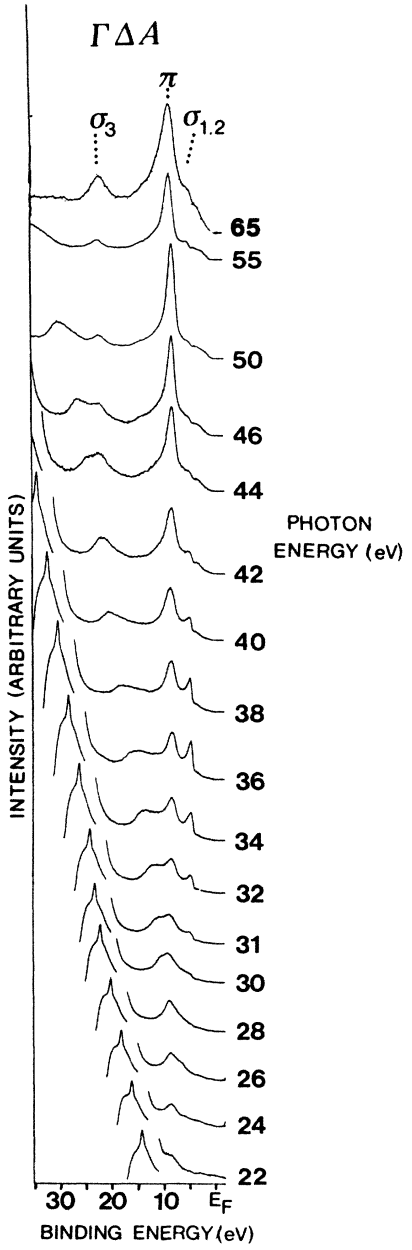

FIG. 8. Energy distribution curves recorded at normal emission as a function of photon energy. The strong features moving to higher binding energy as the photon energy is increased, i.e., appearing at constant kinetic energy, correspond to secondary-electron emission from conduction bands at 7.6 and ~21 eV above the Fermi level.

~3 eV KE, as suggested by Oelhafen and Freeouf.[26] This is assumed to lie at 7.6 eV above E_F. The measured work function is 4.7±0.2 eV.

Emission from the π valence band emerges from the secondary tail background at $h\nu \sim 22$ eV. Between $h\nu = 26$ eV and 32 eV the π band moves up through the Γ_4^- σ^* conduction band lying ~21 eV above E_F, already observed as a prominent secondary feature in the 35 eV and 65 eV spectra. This σ^* conduction band is then observed strongly at fixed kinetic energy for higher photon energies. Emission from the degenerate σ_1,σ_2 valence bands does not become distinct until $h\nu > 30$ eV, after which its intensity increases to a maximum at $h\nu \sim 36$ eV and then drops off, making determination of the binding energy difficult at higher photon energies. Emission from the bottom of the valence band is first observed at $h\nu = 42$ eV when electrons from the σ_3 band are excited into the Γ_4^- σ^* conduction band minimum. The σ_3 band then becomes distinct at higher photon energies. As in the 65 eV data this band is observed to lie at a higher binding energy than calculated.

The dominance of the π-band emission over σ_1,σ_2-band emission in the spectra at high photon energies (as also observed by McGovern *et al.*[6] for $h\nu = 40$ and 50 eV, normal emission ARUPS from HOPG) can be explained by consideration of the parent atomic orbitals constituting the valence bands. If the final state is assumed to be a single plane wave, then the photoexcitation matrix element reflects the angular distribution of the parent atomic orbitals constituting the valence bands, modified by the $|\mathbf{A}\cdot\mathbf{p}|^2$ term.[16] A plane-wave final-state approximation is expected to become more valid at higher energies. Intensity from the π band, resulting from overlap of $2p_z$ orbitals projecting out of the carbon planes, will therefore be stronger than that from the σ-valence bands, whose parent sp hybridized orbitals lie within the plane.

Emission from either the degenerate σ_1 and σ_2 bands or the σ_3 band is not observed for photon energies that would excite electrons from these bands into the calculated band gap lying between 12 and 21 eV above E_F along ΓA. However, emission from the π band is observed for photon energies between 22 and 28 eV, corresponding to final-state energies in this gap. Marchand *et al.*[3] also observe emission from this gap. The π-band emission could result from quasielastic (phonon) scattering from states distributed in other parts of the Brillouin zone. However, such a scattering mechanism does not explain the absence of σ-band emission. As discussed by Willis and Feuerbacher[28] band-gap emission is observed when electrons, excited from initial states to a final-state energy in the gap, match onto the "tails" of vacuum plane waves exponentially decaying into the solid. In fact, such tails exist at all final-state energies. The observation of emission from the π band and not the σ bands implies greater overlap of the vacuum plane-wave tail with the orbitals constituting the π band than with the sp^2 hybridized orbitals constituting the σ bands. This is to be expected since the sp^2 orbital wave functions have zero amplitude in the ΓA direction.

To determine the dispersion of the π band along ΓA the perpendicular component of momentum ($k_{\perp} = 0$ for nor-

mal emission) was calculated according to:[29]

$$k_\perp = [2m(E_{\text{kin}} + V_0)/\hbar^2]^{1/2} , \quad (1)$$

where E_{kin} is the photoelectron kinetic energy and V_0 is the inner potential.

At all photon energies only one peak corresponding to emission from the π band is observed. We have shown[23] that this results from a combination of the symmetry of the detectable final state and the dipole selection rules. Hermanson[19] has shown that for normal emission only final states totally symmetric with respect to symmetry operations about the surface normal will result in measurable intensity at the detector. For cubic crystals only one final state has the appropriate symmetry. For crystals belonging to nonsymmorphic space groups, such as those with the hexagonal-close-packed, diamond, or graphite structures, we have shown[23] that there is more than one final state having the appropriate symmetry. The symmetry of the detectable final state changes with the wave vector (kinetic energy) of the final-state wave function (photoelectron). For graphite either a Δ_1 or Δ_2 symmetry final state can be observed depending on the final-state energy. Dipole selection rules then dictate the accessible initial states.[30] For the experimental configuration employed here, with p-polarized light incident at 45° to the surface normal, the only allowed transitions of interest are $\Delta_1 \rightarrow \Delta_1$, $\Delta_6 \rightarrow \Delta_1$ and $\Delta_2 \rightarrow \Delta_2$, $\Delta_5 \rightarrow \Delta_2$. In theoretical band structures the π bands have Δ_1 and Δ_2 symmetry. The experimentally determined π-band dispersion is shown in Fig. 9. In a preliminary plot of binding energy versus photon energy the observed trend in binding energy of the π-band peak implied a Δ_2-Δ_2-Δ_1 sequence of final-state (and hence initial-state) symmetry, only one final state being accessible at a given photon energy. From the expected theoretical order of the final-state symmetry with final-state energy[31] this observed final-state sequence uniquely determines the value of V_0 in Eq. (1). This is found to be 14.5 ± 1.0 eV, a value that agrees well with that determined from LEED—13 eV.[32]

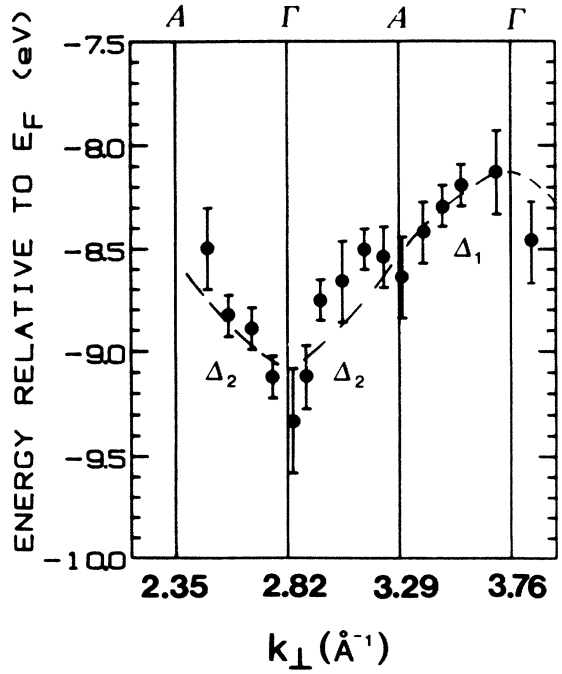

FIG. 9. Binding energy of the observed π peak in the spectra of Fig. 8 as a function of perpendicular momentum $k_\perp$ of the final-state plane wave as given by Eq. (1). The symmetry label of the initial-state band and the uncertainty in the determination of the binding energy are shown.

It can be seen from Fig. 9 that the experimentally determined dispersion is ~ 1 eV. This is less that predicted theoretically—2.0 eV (Ref. 25) and 1.7 eV (Ref. 1)—implying that the interlayer interaction is not as great as calculated. In the theoretical calculations the π-band splitting is sensitive to the crystal potential and exchange-correlation approximation employed. The dispersion determined here is also slightly less than the value of 1.4 eV inferred by Marchand *et al.*[3] from the scatter in the π-band peak position observed in spectra recorded with photon energies between 17 and 27 eV.

V. CONCLUSIONS

To facilitate comparison with both theory and other experimental data Table I lists the experimentally determined binding energies of critical points in the band structure. References 3 and 4 give similar tables, together with the critical-point binding energies calculated in Refs. 1, 11, 25, and 33. When presenting experimental band dispersions we have compared them with the Tatar and Rabii (TR) calculation.[1] This was found to give best overall agreement, though the valence-band dispersions and binding energies given by the various theoretical methods are very similar.

The observed total valence-band width, ~ 21 eV, is greater than that calculated by TR and agrees better with the Holzwarth, Louie, and Rabii (HLR) (Ref. 25) calculation using a Slater exchange-correlation potential. The HLR calculation[25] also gives better agreement with the observed binding energy of the π bands, but predicts a greater dispersion along ΓA, than observed. The HLR calculation also places the top σ valence bands, σ_1, σ_2, at around 1 eV to lower binding energy than where it is observed, and where predicted by TR (Ref. 1) and Willis, Fitton, and Painter (WFP).[11]

Greater discrepancies between calculations arise over the energy positions of the conduction bands. The differences in conduction-band binding energies as given by photoemission and SEE and inverse photoemission (IPES) were mentioned earlier and have been discussed elsewhere.[21,22] IPES results of Fauster *et al.*[10] showed conduction-band dispersions in agreement with those calculated by HLR (Ref. 25). They observed the Γ_1^+ σ^* conduction band (the interlayer state of Ref. 24) at $+3.6$ eV above E_F and the Γ_5^+, Γ_6^- minima at $+9.5$ eV above E_F. In the TR (Ref. 1) and WFP (Ref. 11) band structures these three bands coincide at $\sim +7.6$ eV above E_F, appearing in photoemission spectra (and electron excited SEE) as the very strong feature at ~ 3 eV kinetic energy. This conduction band is also seen at ~ 3 eV KE by Penning ionization electron spectroscopy.[34] Since HLR (Ref.

TABLE I. Binding energies of bands at critical points in the graphite band structure determined from the 35 eV, 65 eV, and normal-emission data. The symmetry labels of the bands are those of Tatar and Rabii.[a]

Critical point		Photon energy	Binding energy (eV) 35 eV	65 eV	Normal emission
Γ	Γ_4^-,Γ_1^+	σ_3	...	21.0	22.3±0.2
	Γ_3^+				9.1±0.2
		π	8.0	8.0	8.5±0.2 (A_1)
	Γ_2^-				8.1±0.2
	Γ_6^-,Γ_5^+	$\sigma_1\sigma_2$	4.5	4.0	5.0±0.2
	$\Gamma_{11}^+\Gamma_5^+,\Gamma_6^-$	σ^*	$E_F+7.2$	$E_F+7.7$	$E_F+7.6$
	Γ_3^+,Γ_2^-	π^*	$E_F+10.7$	...	...
	Γ_4^-	σ^*	$E_F+21.0$	$E_F+20.2$	$E_F+20.1\pm0.2$
M	M_1^+,M_2^-	σ_3	15.6	14.0	
	M_2^-,M_1^+	σ_2	14.3		
	M_3^-,M_4^+	σ_1	7.8	7.0	
	M_3^+,M_4^-	π	2.8	2.5	
K	K_1,K_3,K_5	σ_2,σ_3	14.5	14.0	
	K_5	σ_1	11.5	11.0	
	K_2,K_6	π	0.6	0.7,0.25	

[a]Reference 1.

25) only calculate the conduction bands up to 12.5 eV above E_F, the other prominent SEE features can only be compared with the TR (Ref. 1) calculation and with the WFP (Ref. 11) calculation, where the conduction bands are calculated up to 55 eV above E_F. The TR band structure agrees well with the experimental dispersion of both the fairly flat Γ_4^- σ^* band and the highly dispersive π^* band along ΓK. The WFP calculation places the σ^* band correctly, but wrongly predicts the dispersion of the π^* band, placing the band ~ 10 eV higher in energy at K.

In conclusion, we have fully determined the valence-band dispersions and critical-point binding energies of the graphite band structure. In addition, distinct secondary-electron features in the photoemission spectra allow determination of the dispersion of conduction bands lying up to ~ 20 eV above the Fermi level. Such high-energy features are not observed in IPES due to final-state broadening effects. Our results give best overall agreement with the modified KKR calculation of Tatar and Rabii.[1]

ACKNOWLEDGMENTS

Two of us (A.R.L.) and (M.T.J.) gratefully acknowledge the support of the United Kingdom Science and Engineering Research Council. We acknowledge D. Pescia and H. I. Starnberg for stimulating discussions, and H. A. Padmore and D. Norman for their assistance during the experimental part of this work.

[1]R. C. Tatar and S. Rabii, Phys. Rev. B **25**, 4126 (1982).
[2]F. R. McFeely, S. P. Kowalczyk, L. Ley, R. G. Cavell, R. A. Pollak, and D. A. Shirley, Phys. Rev. B **9**, 5268 (1974).
[3]D. Marchand, C. Fretigny, M. Lagues, F. Batallan, Ch. Simon, I. Rosenman, and R. Pinchaux, Phys. Rev. B **30**, 4788 (1984).
[4]T. Takahashi, H. Tokailin, and T. Sagawa, Solid State Commun. **52**, 765 (1984).
[5]A. R. Law, J. J. Barry, and H. P. Hughes, Phys. Rev. B **28**, 5332 (1983).
[6]I. T. McGovern, W. Eberhardt, E. W. Plummer, and J. E. Fischer, Physica **99B**, 415 (1980).
[7]P. M. Williams, D. Latham, and J. Wood, J. Electron Spectrosc. Rela. Phenom. **7**, 281 (1975).
[8]R. F. Willis, B. Feuerbacher, and B. Fitton, Phys. Rev. B **4**, 2441 (1971).
[9]V. Dose, G. Reusing, and H. Scheidt, Phys. Rev. B **26**, 984 (1982).
[10]Th. Fauster, F. J. Himpsel, J. E. Fischer, and E. W. Plummer, Phys. Rev. Lett. **51**, 470 (1983).
[11]R. F. Willis, B. Fitton, and G. S. Painter, Phys. Rev. B **9**, 1926 (1974).
[12]L. S. Caputi, G. Chiarello, E. Colavita, A. Santaniello, and L. Papagno, Surf. Sci. **152-153**, 278 (1985).
[13]L. Papagno and L. S. Caputi, Surf. Sci. **125**, 530 (1983).
[14]D. L. Greenaway, G. Harbeke, F. Bassani, and E. Tossati, Phys. Rev. **178**, 1340 (1969).
[15]H. P. Hughes and W. Y. Liang, J. Phys. C **6**, 1684 (1973).
[16]N. V. Smith, in *Photoemission in Solids I*, edited by M. Cardona and L. Ley (Springer-Verlag, Berlin, 1978).
[17]R. H. Williams, G. P. Srivastarva, and I. T. McGovern, Rep. Prog. Phys. **43**, 1357 (1980).
[18]E. Dietz and D. E. Eastman, Phys. Rev. Lett. **41**, 1674 (1978).
[19]J. Hermanson, Solid State Commun. **22**, 9 (1977).
[20]B. Feuerbacher and R. F. Willis, J. Phys. C **9**, 169 (1976).
[21]A. R. Law, M. T. Johnson, H. P. Hughes, and H. A. Padmore, J. Phys. C **18**, L297 (1985).

[22]M. T. Johnson, A. R. Law, and H. P. Hughes, Surf. Sci. **162**, 11 (1985).
[23]D. Pescia, A. R. Law, M. T. Johnson, and H. P. Hughes, Solid State Commun. **56**, 809 (1985).
[24]M. Posternak, A. Baldereschi, A. J. Freeman, E. Wimmer, and M. Weinert, Phys. Rev. Lett. **50**, 761 (1983).
[25]N. A. W. Holzwarth, S. G. Louie, and S. Rabii, Phys. Rev. B **26**, 5382 (1982).
[26]P. Oelhafen and J. L. Freeouf, J. Vac. Sci. Technol. A **1**, 96 (1983).
[27]J. Kreig, P. Oelhafen, and H.-J. Güntherodt, Solid State Commun. **42**, 831 (1982).
[28]R. F. Willis and B. Feuerbacher, in *Photoemission and the Electronic Properties of Surfaces,* edited by B. Feuerbacher, B. Fitton, and R. F. Willis (Wiley, Chichester, 1978).
[29]F. J. Himpsel, Adv. Phys. **32**, 1 (1983).
[30]R. L. Benbow, Phys. Rev. B **22**, 3775 (1980).
[31]J. C. Slater, *Quantum Theory of Molecules and Solids* (McGraw-Hill, New York, 1965), Vol. 2, p. 467 Figure A7-1.
[32]J. J. Lander and J. Morrison, J. Appl. Phys. **35**, 3593 (1964).
[33]C. P. Mallett, J. Phys. C **14**, L213 (1981).
[34]Y. Harada, H. Ozaki, and K. Ohno, Phys. Rev. Lett. **52**, 2269 (1984).